Shiga toxin–binding site for host cell receptor GPP130 reveals unexpected divergence in toxin-trafficking mechanisms

Somshuvra Mukhopadhyay*, Brendan Redler, and Adam D. Linstedt
Department of Biological Sciences, Carnegie Mellon University, Pittsburgh, PA 15213

ABSTRACT **Shiga toxicosis is caused by retrograde trafficking of one of three types of Shiga toxin (STx), STx, STx1, or STx2. Trafficking depends on the toxin B subunits, which for STx and STx1 are identical and bind GPP130, a manganese (Mn)-sensitive intracellular trafficking receptor. Elevated Mn down-regulates GPP130, rendering STx/STx1 harmless. Its effectiveness against STx2, however, which is a serious concern in the developed world, is not known. Here we show that Mn-induced GPP130 down-regulation fails to block STx2 trafficking. To shed light on this result, we tested the purified B subunit of STx2 for binding to GPP130 and found that it failed to interact. We then mapped residues at the interface of the GPP130-STx/STx1 complex. In GPP130, binding mapped to a seven-residue stretch in its lumenal stem domain next to the transmembrane domain. This stretch was required for STx/STx1 transport. In STx/STx1, binding mapped to a histidine–asparagine pair on a surface-exposed loop of the toxin B subunit. Significantly, these residues are not conserved in STx2, explaining the lack of effectiveness of Mn against STx2. Together our results imply that STx2 uses an evolutionarily distinct trafficking mechanism and that Mn as a potential therapy should be focused on STx/STx1 outbreaks, which account for the vast majority of cases worldwide.**

Monitoring Editor
Benjamin S. Glick
University of Chicago

Received: Jan 28, 2013
Revised: May 31, 2013
Accepted: Jun 3, 2013

INTRODUCTION

Shiga toxin–producing bacteria of the *Shigella* genus and *Escherichia coli* strains are a major cause of food- and water-borne disease in the world (O'Brien and Holmes, 1987; Kotloff *et al.*, 1999; Reller and Griffin, 2004). The toxin produced by *Shigella* is called Shiga toxin (STx). STx production is most commonly associated with *Shigella dysenteriae*, but STx production at lower levels occurs in other *Shigella* species, and severity of *Shigella*-induced disease has been correlated to the production of STx (Keusch and Jacewicz, 1977; O'Brien *et al.*, 1977; Fontaine *et al.*, 1988). Annually, *Shigella* infect >164 million people and cause >1 million deaths, with >99% of these infections occurring in developing countries (Kotloff *et al.*, 1999). Two related toxins, STx1 and STx2, are produced by specific *E. coli* strains (called Shiga toxin–producing *E. coli* [STEC]; Strockbine *et al.*, 1988). In contrast to *Shigella*, STEC infections primarily occur in developed countries and affect far fewer individuals (annual incidence of ~70,000 in the United States; Nataro and Pickering, 2006; Mohawk and O'Brien, 2011). STx1 is nearly identical to STx, with 100% identity in the B subunit and a single conservative amino acid change in the A subunit (Strockbine *et al.*, 1988). In contrast, STx2 shares only ~55% sequence identity with STx (Strockbine *et al.*, 1988), and the production of STx2 correlates with severe disease phenotypes (Tesh *et al.*, 1993; Boerlin *et al.*, 1999; Tam *et al.*, 2008). All three toxins use a common mechanism in inducing cell death by blocking protein synthesis (O'Brien and Holmes, 1987), and, despite the sequence divergence, STx2 undergoes retrograde transport similar to STx and STx1 (Tam *et al.*, 2008).

Retrograde trafficking in host cells begins with the association of the toxin B subunit with the lipid Gb3 on the cell surface, followed by internalization to early endosomes (Mallard *et al.*, 1998; Johannes and Popoff, 2008; Beddoe *et al.*, 2010). In early endosomes STx/STx1 binds the membrane protein GPP130, which directs it to the

This article was published online ahead of print in MBoC in Press (http://www.molbiolcell.org/cgi/doi/10.1091/mbc.E13-01-0057) on June 12, 2013.

*Present address: Division of Pharmacology & Toxicology, College of Pharmacy; Institute for Cellular & Molecular Biology; and Institute for Neuroscience, University of Texas at Austin, Austin, TX 78712.

Address correspondence to: Adam D. Linstedt (linstedt@cmu.edu).

Abbreviations used: GFP, green fluorescent protein; GST, glutathione *S*-transferase; Mn, manganese; PBS, phosphate-buffered saline; PMSF, phenylmethylsulfonyl fluoride; STEC, Shiga toxin–producing *Escherichia coli*; STx, Shiga toxin; STx1, Shiga toxin 1; STx2, Shiga toxin 2.

© 2013 Mukhopadhyay *et al.* This article is distributed by The American Society for Cell Biology under license from the author(s). Two months after publication it is available to the public under an Attribution–Noncommercial–Share Alike 3.0 Unported Creative Commons License (http://creativecommons.org/licenses/by-nc-sa/3.0).

"ASCB®," "The American Society for Cell Biology®," and "Molecular Biology of the Cell®" are registered trademarks of The American Society of Cell Biology.

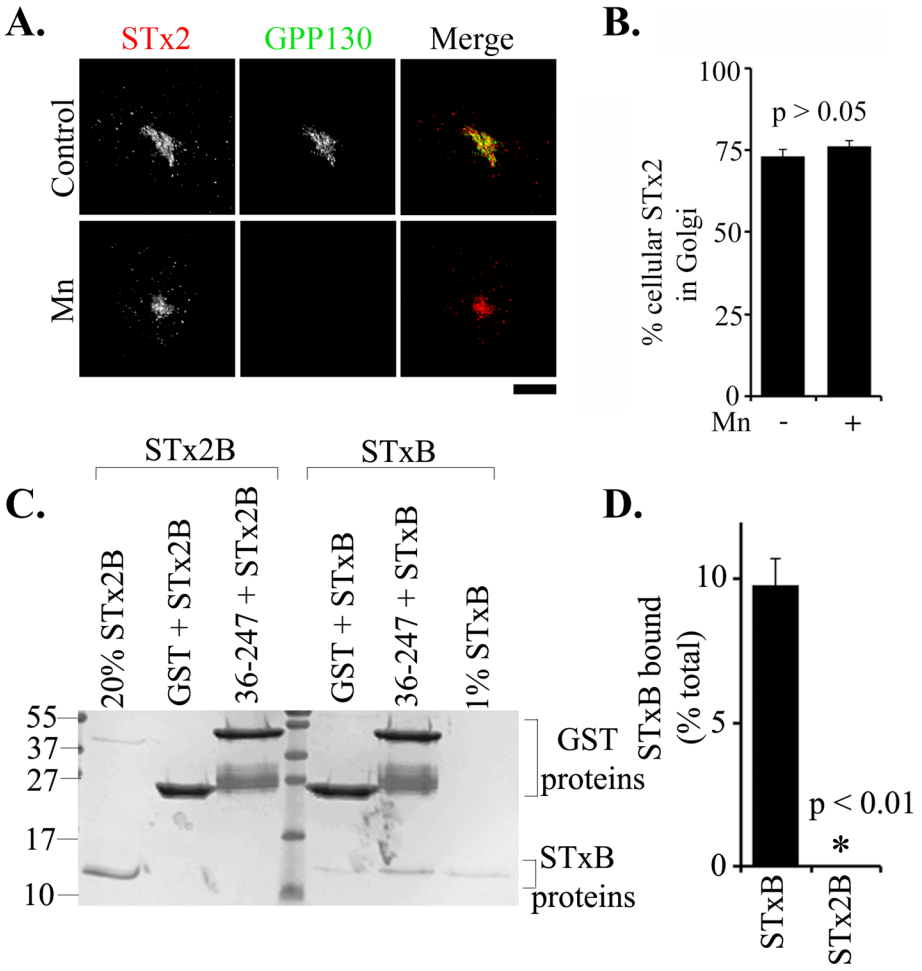

FIGURE 1: Retrograde transport of STx2 is GPP130 independent. (A) HeLa cells were transfected with untagged Gb3 synthase and after 2 d were exposed to 500 μM Mn for 4 h or left untreated. The STx2 transport assay was then performed as described in *Materials and Methods*. Immunofluorescence was used to detect STx2 (red) and GPP130 (green). Scale bar, 5 μm. (B) Percentage of total cellular STx2 in the Golgi was quantified for cells fixed 30 min after initiation of STx2 transport. See *Materials and Methods* for details. Mean ± SE; $n = 51$ cells per group; $p > 0.05$. (C, D) Coomassie-stained gels and quantified recovery of the binding of His-tagged full-length STxB and full-length STx2B to GST-GPP130$_{36\text{-}247}$ or GST-only control. Binding assays were performed using 5 μM GST proteins and 0.4 μM STxB or STx2B ($n = 3$, $p < 0.01$).

Golgi apparatus (Mukhopadhyay and Linstedt, 2012). Direct trafficking from early endosomes to the Golgi, bypassing late endosomes and lysosomes, is a crucial step, as it allows STx/STx1 to avoid exposure to the degradative action of hydrolases that are active in these organelles. GPP130 is an integral membrane protein that constitutively traffics between the Golgi apparatus and early endosomes (Linstedt *et al.*, 1997; Bachert *et al.*, 2001). Appearance of STx/STx1 in Golgi-directed membrane tubules that extend from early endosomes depends on its direct interaction with the GPP130 lumenal domain (Mukhopadhyay and Linstedt, 2012). Although the normal function of GPP130 is unclear, elevated manganese (Mn) diverts GPP130 to lysosomes, causing its degradation (Mukhopadhyay *et al.*, 2010). Because STx/STx1 trafficking depends on GPP130, Mn-induced GPP130 down-regulation renders STx/STx1 harmless by rerouting it to lysosomes, where it is degraded along with other toxic agents that invade cells (Mukhopadhyay and Linstedt, 2012). In tissue culture cells, treatment with Mn yields a 3800-fold protection against STx1-induced cell death. Mice injected with nontoxic doses of Mn are completely resistant to lethal STx1 challenges. These findings strongly suggest that Mn represents an unexpected, low-cost therapeutic agent for STx/STx1 treatment.

Whether STx2 is also susceptible to Mn treatment is unknown. This is an important question because of the severity and prevalence of STx2 in outbreaks within developed nations, which are significant, albeit minor in comparison to the number of individuals affected by STx. Here we address this question and report that unlike STx/STx1, STx2 is insensitive to Mn. Further experiments elucidate the mechanism. STx2 neither binds GPP130 nor depends on GPP130 for its trafficking. Mapping of the B subunit and GPP130 residues mediating binding identified a histidine/asparagine pair critical for STx/STx1 binding to GPP130 but lacking in STx2. In sum, STx2 evolved an evolutionarily distinct trafficking mechanism such that Mn sensitivity is specific to STx and STx1 toxin types.

RESULTS

Manganese sensitivity of STx2 trafficking

To test the manganese sensitivity of STx2 trafficking, we carried out a previously established trafficking assay in HeLa cells using fluorescently labeled holotoxin (Mukhopadhyay and Linstedt, 2012). As expected, STx2 efficiently trafficked to the Golgi in control cells (Figure 1A). To our surprise, when the same experiment was carried out in cells treated for 4 h with 500 μM $MnCl_2$, a condition that potently blocks STx/STx1 B-subunit trafficking (Mukhopadhyay and Linstedt, 2012; see later discussion of Figure 3), STx2 trafficked to the Golgi complex in a manner indistinguishable from the control cells (Figure 1A). Because GPP130 is the relevant target of Mn (Mukhopadhyay and Linstedt, 2012), we confirmed that GPP130 was down-regulated in these experiments by staining the same cells to detect GPP130. As expected, GPP130 was clearly evident in untreated controls and potently depleted in Mn-treated cells (Figure 1A). The quantified levels of STx2 fluorescence in the Golgi confirmed the lack of sensitivity of STx2 to the Mn treatment (Figure 1B).

Comparison of GPP130 binding to STx/STx1 and STx2 B subunits

To test the possibility that the Mn insensitivity of STx2 was due to a lack of interaction with GPP130, we purified the B subunits of STx and STx2 and compared their binding to a purified, glutathione *S*-transferase (GST)–tagged GPP130 construct. In previous work this construct bound STxB, yielding a K_d of 150 nM (Mukhopadhyay and Linstedt, 2012). Consistent with this, nearly 10% of the added STxB bound GPP130 (Figure 1, C and D). In contrast, there was no detectable recovery of STx2B (Figure 1, C and D). Thus, unlike STx/STx1, the B subunit of STx2 did not appear to interact with

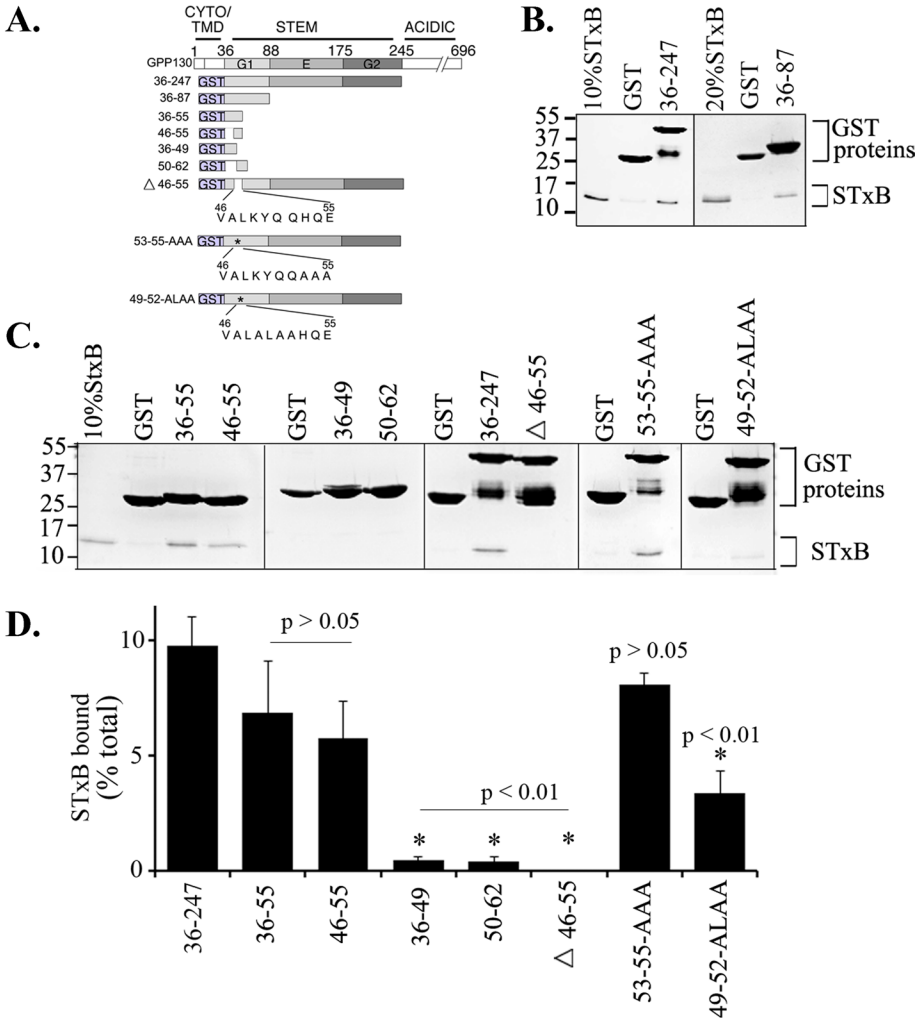

FIGURE 2: Residues 46–55 of GPP130 are necessary and sufficient to interact with STxB. (A) Schematic of GST-tagged GPP130 constructs used in the binding assays. (B–D) Coomassie-stained gels and quantitation for His-STxB recovery after incubation with the indicated GST-tagged GPP130 constructs or GST-only control (mean ± SE; $n = 3$ experiments; p values are for the comparison for each individual GST-GPP130 deletion construct with GST-GPP130$_{36\text{-}247}$ that contains the entire stem domain of GPP130). The data set for GST-GPP130$_{36\text{-}247}$ plotted here is also shown in Figure 1D.

GPP130, providing a plausible explanation for its Mn-insensitive trafficking.

The juxtamembrane sequence VALKYQQ in the GPP130 stem domain mediates binding to the B subunit of STx/STx1

To learn why STx2 failed to interact with GPP130, we sought to elucidate the basis of STx/STx1 binding to GPP130. First, we mapped the STx/STx1-binding site in GPP130. GPP130 has a short cytoplasmic domain, a single transmembrane domain, and a two-part lumenal domain in which the first 210 residues form a coiled-coil stem and the final 451 residues are enriched in acidic amino acids (Figure 2A). The stem of GPP130 can be further subdivided into three subdomains: residues 36–87 and 176–245, which confer Golgi localization, and residues 88–175, which mediate endosome-to-Golgi cycling (Bachert *et al.*, 2001). Prior work (Mukhopadhyay and Linstedt, 2012) showed that STxB binds the GPP130 stem domain (36–245) and that binding occurs in the membrane-proximal subdomain (residues 36–87). Therefore we generated and purified a set of GST-tagged GPP130 deletion constructs (Figure 2A) and tested the ability of these constructs to interact with purified, histidine (His)-tagged, full-length STxB. As expected, GST-GPP130$_{36\text{-}247}$ and GST-GPP130$_{36\text{-}87}$ bound STxB (Figure 2B). We then observed that GST-GPP130$_{36\text{-}55}$ bound STxB at a level comparable to that of the entire stem domain, indicating that the toxin-binding domain lay in the first 20 residues of the stem domain (Figure 2, C and D). Further analyses revealed that a 10–amino acid fragment extending between residues 46 and 55 of GPP130 was sufficient to interact with STxB, whereas residues 36–49 and 50–62 failed to interact (Figure 2, C and D). Deletion of residues 46–55 from the GPP130 stem domain (GST-GPP130$\Delta_{46\text{-}55}$) abolished the GPP130-STxB interaction, indicating that residues 46–55 were also required (Figure 2, C and D). Thus the sequence VALKYQQHQE corresponding to residues 46–55 was necessary and sufficient for STxB binding. As a further test, we substituted residues in two parts of this sequence within the GPP130 stem domain construct (Figure 2A). Alanine substitutions of the HQE stretch (GST$_{53\text{-}55\text{-}AAA}$) did not affect STxB binding, but substitution of the KYQQ stretch with ALAA (GST$_{49\text{-}52\text{-}ALAA}$) significantly reduced binding (Figure 2, C and D). We conclude that the binding site maps to the sequence VALKYQQ situated in the lumenal stem domain ~11 residues distant from the membrane. In common with the entire stem domain, this sequence stretch is highly conserved across at least 20 mammalian species.

The STxB/STx1B-binding domain of GPP130 is required for retrograde toxin transport

To test the functional significance of the mapped binding site in GPP130, we used a complementation approach. We previously showed that the Mn-induced block in STxB transport is reversed by expression of an Mn-insensitive GPP130 construct (Mukhopadhyay and Linstedt, 2012). This construct, GPP130$_{1\text{-}175}$–green fluorescent protein (GFP), was created by truncation of GPP130 after residue 175 to remove a determinant required for the Mn response but leaving targeting, cycling, and STxB-binding functions intact (Mukhopadhyay *et al.*, 2010; Mukhopadhyay and Linstedt, 2012). Therefore our goal was to assay STxB transport in Mn-treated cells expressing the Mn-insensitive version of GPP130 containing a further specific deletion of the mapped STxB-binding site (Figure 3A). First, we verified that the Mn-induced loss of GPP130 blocked STxB transport in the assays. In control cells, STxB efficiently trafficked to the Golgi from the cell surface (Figure 3, B and D). Exposure of cells to 500 μM Mn induced degradation of GPP130, and STxB remained trapped in endosomal punctae rather than trafficking to the Golgi (Figure 3, B and D). Next we confirmed that the wild type, Mn-insensitive construct GPP130$_{1\text{-}175}$-GFP restored STxB transport to the Golgi in Mn-treated cells. In agreement with previous work (Mukhopadhyay and Linstedt,

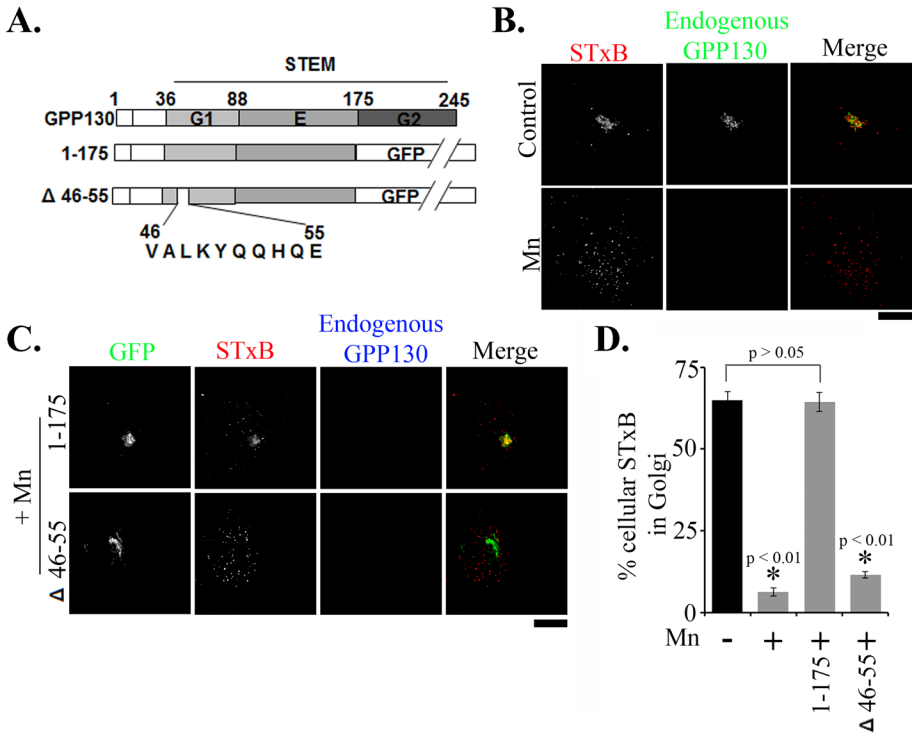

FIGURE 3: The STxB-binding domain of GPP130 is required for endosome-to-Golgi transport of STxB. (A) Schematic of GFP-tagged constructs used in the transport assays. (B) HeLa cells expressing untagged Gb3 synthase for 2 d were treated with or without 500 μM Mn for 4 h. The STxB transport assay was then performed using Alexa Fluor 555–labeled STxB for 30 min as described in *Materials and Methods*. Cultures were processed for immunofluorescence to detect STxB (red) and GPP130 (green). Scale bar, 5 μm (C) HeLa cells cotransfected with untagged Gb3 synthase and the indicated GFP-tagged GPP130 constructs were untreated or treated with 500 μM Mn for 4 h before STxB transport for 30 min (as in B) and imaged to detect GFP (green), STxB (red), and anti–endogenous GPP130 staining (blue). Note that the anti-GPP130 antibody binds the acidic domain that is missing in the transfected constructs. Scale bar, 5 μm. (D) Percentage cellular STxB in the Golgi from B and C (mean ± SE; $n = 38$ cells per group; p values are for the comparison for each group with the no-Mn control group of B).

2012), STxB Golgi transport was restored to the level observed for untreated cells (Figure 3, C and D). Finally, we deleted residues 46–55 from GPP130$_{1\text{-}175}$-GFP and repeated the assay. Significantly, GPP130$\Delta_{46\text{-}55}$-GFP failed to restore STxB transport, and, in these cells, STxB remained trapped in punctate structures (Figure 3, C and D). The GFP-tagged proteins expressed by these constructs were well localized to the Golgi and not degraded upon Mn treatment, whereas endogenous GPP130 was degraded in the same cells, as confirmed using an antibody against the acidic domain of GPP130 that is not present in the GFP-tagged proteins (Figure 3C). Thus the STxB-binding domain of GPP130 encompassed by residues 46–55 is required to support the endosome-to-Golgi transport of STxB. Overall the data suggest that direct interaction of STxB with this site in GPP130 is essential for endosomal sorting and Golgi transport of STxB.

Nonconserved residues $H_{78}N_{79}$ of STxB/STx1B mediate binding to GPP130

To map the GPP130-binding site on STxB, we used the known crystal structure of STxB (Ling *et al.*, 1998) and considered the likely orientation of STxB on the membrane when bound to its lipid receptor Gb3. We then targeted regions on the resulting exposed sidewall of STxB using amino acid substitutions in an attempt to block binding to GPP130. Most of those tested had little or no effect, but when we introduced three substitutions (K73E, H78A, N79A) into a surface-exposed loop of the toxin, we observed a strong loss of the interaction (Figure 4, A–D). Of interest, this loop of STxB is a prominent feature almost certainly accessible to the mapped binding site of GPP130, given the latter's proximity to the membrane. Because the histidine–asparagine pair (positions 78 and 79) could potentially hydrogen bond with the tandem glutamines in GPP130, we next generated a double mutant (H78A, N79A). Binding of the H78A-N79A double mutant was also markedly blocked and did not significantly differ from that of the triple mutant (Figure 4, C and D). Thus the GPP130-binding interface of STxB mapped to the histidine–asparagine pair on a surface-exposed loop of the toxin.

To test the functional significance of the mapped binding site, we compared retrograde transport of STxB wild type to the double mutant STxB$_{H78A\text{-}N79A}$. Whereas STxB wild type trafficked to the Golgi, STxB$_{H78A\text{-}N79A}$ accumulated in peripheral punctae, indicating that it underwent endocytosis but not Golgi trafficking (Figure 4E). Quantification confirmed a profound block in trafficking to the Golgi (Figure 4F). Thus the binding-site residues are functionally required, and their discovery led to novel point mutations in the toxin that block its ability to invade cells.

Significantly, the histidine–asparagine pair present in STxB/STx1B is not conserved in the B subunit of STx2 (STx2B) or any of its known subtypes (Figure 5). In fact, instead of the histidine at this position, STx2B has a glutamic acid, implying a significant change in charge characteristics (Figure 5). Thus our experiments document the Mn insensitivity of STx2 trafficking and reveal the underlying cause to be an unexpected lack of conservation in key residues that in STx and STx1 mediate their interaction with the intracellular trafficking receptor GPP130.

DISCUSSION

Direct transport from early endosomes to the Golgi apparatus protects Shiga toxins from degradation and is essential for productive infections. Targeting this transport step is therapeutically appealing, but the underlying cellular machinery is only now being revealed. Sorting of these toxins in early endosomes into Golgi-directed tubules requires communication between the lumenal toxin and the cytosolic trafficking machinery. For STx/STx1, this is achieved, at least in part, by the direct binding of its B subunit to the lumenal domain of GPP130. This binding allows the toxin to exploit the trafficking itinerary of a host protein that cycles between early endosomes and the Golgi. Significantly, blocking this interaction diverts the toxin to lysosomes, where it is degraded (Mukhopadhyay and Linstedt, 2012). Here we identify key residues at the STxB-GPP130 interface. Although the binding site in GPP130 is highly conserved, the $H_{78}N_{79}$ motif of STx/STx1 is not conserved in STx2. Indeed, STx2 neither bound GPP130 nor depended on GPP130 for its

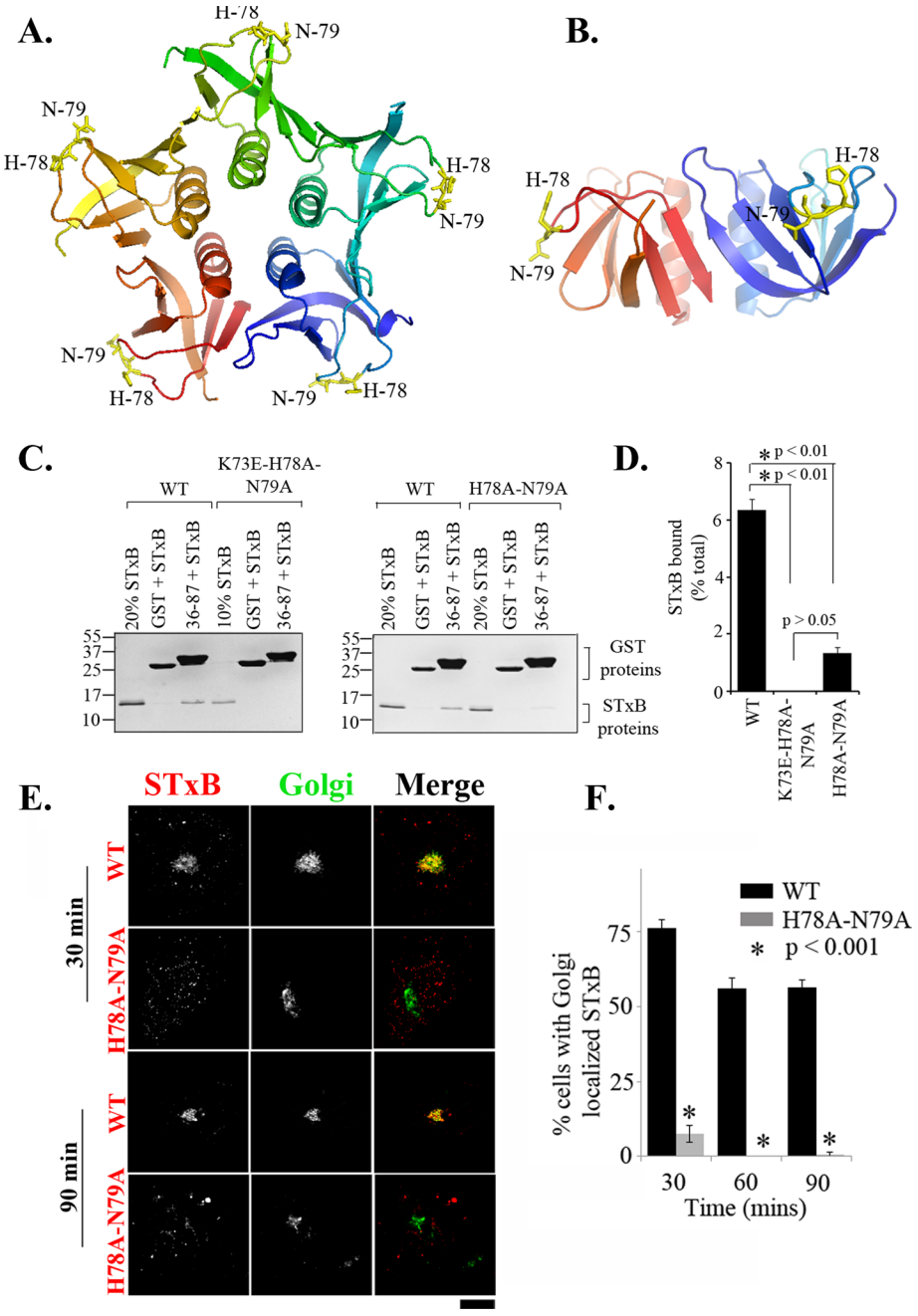

FIGURE 4: Surface-exposed STxB residues H-78 and N-79 are required for GPP130 binding and retrograde transport to the Golgi. (A, B) Crystal structure of STxB (PDB ID 1BOS; Ling *et al.*, 1998) in cartoon format with surface-exposed residues H-78 and N-79 in stick format. (B) Highlighted residues are on the sidewall, and the membrane-binding surface is on top. (C, D). Coomassie-stained gels and quantified recovery of various His-STxB proteins after incubation with GST-GPP130$_{36\text{-}87}$, which contains the STxB-binding domain, or GST only. Binding was carried out as described in *Materials and Methods* using 5 μM GST proteins and 0.4 μM STxB (mean ± SE; $n = 3$ experiments; one-way ANOVA with Tukey–Kramer post hoc test revealed that there was statistically significant difference between STxB wild type [WT] and STxB$_{K73E\text{-}H78A\text{-}N79A}$, and STxB-WT and STxB$_{H78A\text{-}N79A}$ [$p < 0.01$ for both comparisons] but not between STxB$_{K73E\text{-}H78A\text{-}N79A}$ and STxB$_{H78A\text{-}N79A}$ [$p > 0.05$]). (E) HeLa cells expressing GFP-tagged Gb3 synthase for 2 d were incubated with Alexa Fluor 555–tagged STxB wild type (WT) and the $H_{78}A\text{-}N_{79}A$ double mutant and analyzed for transport after 30, 60, or 90 min as described in *Materials and Methods*. Shown are STxB proteins (red) and Gb3 synthase, to demarcate the Golgi (green). Scale bar, 5 μm. F. The percentage of cells with Golgi-localized STxB wild type (WT) or STxB $H_{78}A\text{-}N_{79}A$ was quantified at each time point by counting ($n = 3$, >30 cells each construct per time point per experiment, $p < 0.001$).

trafficking to the Golgi complex. These results reveal a significant functional divergence in Shiga toxin evolution.

The GPP130 independence of STx2 trafficking implies the presence of a distinct mechanism mediating its sorting in early endosomes. This finding is consistent with an earlier study comparing retrograde transport of STx1 and STx2 in which the toxins only partially colocalized with one another in endosomes and STx2 was more susceptible to detergent extraction (Tam *et al.*, 2008). It might also explain, at least in part, the enhanced in vivo toxicity of STx2 relative to STx1 (Tesh *et al.*, 1993; Boerlin *et al.*, 1999; Tam *et al.*, 2008). That is, it is conceivable that by using a different intracellular trafficking receptor the efficiency of STx2 sorting and/or endosome-to-Golgi transport may be superior, thereby producing a greater toxic load. Numerous transport factors have been identified that mediate endosomal sorting and Golgi transport of STx/STx1 (Johannes and Popoff, 2008; Johannes and Wunder, 2011). It is now important to determine which of these, if any, also mediate STx2 transit.

GPP130 is the only endosomal receptor identified for AB_5 toxins, the category of toxins, including the Shiga toxins, that have a single A subunit associated with five B subunits. Because these toxins share broad thematic similarities in their retrograde transport, an important implication of our work is that other AB_5 toxins, including STx2, may similarly coopt different host proteins that traffic from endosomes to the Golgi. Characteristics of GPP130 and its STx/STx1 binding interface may lead to discovery of related receptors and the ability to counter disease caused by STx2, cholera, and other toxins.

Lipid-based sorting is also believed to contribute to retrograde transport of AB_5 toxins (Falguieres *et al.*, 2001; Chinnapen *et al.*, 2012). For example, STx/STx1 is detected in detergent-resistant membranes, and cholesterol depletion blocks the retrograde transport of STx (Falguieres *et al.*, 2001). GPP130 has a longer transmembrane domain than typical Golgi proteins, which may promote its inclusion in cholesterol-enriched membrane microdomains (Bretscher and Munro, 1993). Thus binding to GPP130 may concentrate STx/STx1 in these domains. The STx/STx1 glycosphingolipid receptor Gb3 also associates with cholesterol-enriched domains (Falguieres *et al.*, 2001). Because the $H_{78}N_{79}$ motif that mediates the STx/STx1-GPP130 interaction is separate from the binding site for Gb3 (Ling *et al.*, 1998), STx/STx1 could

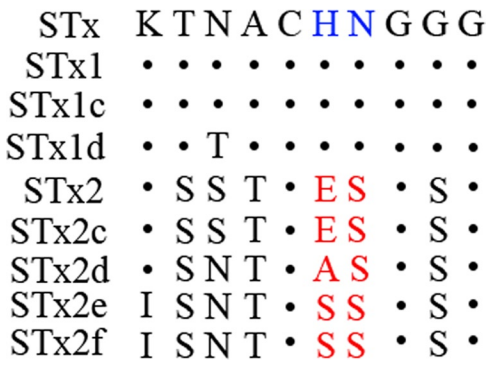

FIGURE 5: Lack of conservation of STxB residues H-78 and N-79. Sequence alignment of the surface-exposed loop of STxB/STx1B that constitutes the GPP130-binding site. Residues H78 and N79 in STxB are highlighted in blue. Comparison includes STx (Strockbine *et al.*, 1988); STx1, STx1c, and STx1d (Burk *et al.*, 2003); STx2 and STx2c (Schmitt *et al.*, 1991); STx2d (Zhang *et al.*, 2005); STx2e (Weinstein *et al.*, 1988); and STx2f (Gannon *et al.*, 1990).

simultaneously interact with GPP130 and Gb3, strengthening its association with specialized microdomains. A critical question is how the STx-GPP130 complex engages cytosolic trafficking machinery. In principle, any component of a putative STx-GPP130–containing microdomain might be responsible. Nevertheless, it will be important to test for direct interaction of GPP130's cytoplasmic domain with transport factors implicated in endosome-to-Golgi transport and then extend our knowledge to endosomal sorting of other AB_5 toxins.

Shigella bacteria that produce STx, and not STx1 or 2, cause the vast majority of Shiga toxicosis cases worldwide. An implication of our work is that agents that target GPP130 are likely to be therapeutically useful for the management of these infections. Indeed, treatment with Mn to reduce GPP130 provides >3800-fold protection against toxin-induced cell death in culture and complete protection in mice (Mukhopadhyay and Linstedt, 2012). Although chronic exposure to elevated Mn is neurotoxic (Aschner *et al.*, 2009), the protection against STx1 in cells and mice requires only brief Mn exposures that elicit no detectable toxicity (Mukhopadhyay and Linstedt, 2012). Thus the possibility of using Mn for treatment of STx infections is promising. Further, our mapping of the interface involved in the GPP130-STxB interaction provides important information for the design of additional inhibitors to protect against STx-induced disease.

MATERIALS AND METHODS

Constructs, antibodies, and chemicals

Generation of a GST-tagged GPP130 construct that contains the entire lumenal domain of GPP130 has been described (Mukhopadhyay and Linstedt, 2012). A GFP-tagged GPP130 construct containing residues 1–175 of GPP130 has also been described (Mukhopadhyay and Linstedt, 2012). His-tagged STxB used for the binding assays was a gift of Mark Stamnes (University of Iowa, Iowa City, IA) and was previously described (Mukhopadhyay and Linstedt, 2012). Deletion and point mutations were introduced into the foregoing constructs using the QuikChange mutagenesis kit (Agilent Technologies, Santa Clara, CA). Plasmid for STx2B was from Alison Weiss (University of Cincinnati, Cincinnati, OH). STx2 holotoxin and rabbit polyclonal antibody against STx2 were from Clifford Lingwood (Hospital for Sick Children, Toronto, Canada). Unless otherwise noted, all antibodies and chemicals used in this study were previously described (Mukhopadhyay *et al.*, 2010; Mukhopadhyay and Linstedt, 2011, 2012).

Cell culture, transfections, Mn treatment, and immunofluorescence microscopy

These were done essentially as described (Mukhopadhyay *et al.*, 2010; Mukhopadhyay and Linstedt, 2011, 2012). Mn treatment was by adding freshly prepared $MnCl_2$ to the culture medium at 500 μM for 4 h unless otherwise specified. Images were captured with a spinning-disk confocal scan head microscope equipped with three-line laser and independent excitation and emission filter wheels (PerkinElmer Life and Analytical Sciences, Boston, MA) and a 12-bit Orca ER digital camera (Hamamatsu Photonics, Bridgewater, NJ) mounted on an Axiovert 200 microscope with a 100×, 1.4 numerical aperture oil immersion objective (Carl Zeiss, Thornwood, NY) as described previously (Mukhopadhyay *et al.*, 2010; Mukhopadhyay and Linstedt, 2011, 2012). Corresponding images in each experiment were acquired under identical parameters.

Purification and fluorescence tagging of STxB

Untagged STxB was purified essentially as described (Mukhopadhyay and Linstedt, 2012). Briefly, the washed cell pellet from a 1-l culture was resuspended in 30 ml of ice-cold water with 10 μg/ml leupeptin, 10 μg/ml pepstatin, and 1 mM phenylmethylsulfonyl fluoride (PMSF) and, after 10 min on ice, a supernatant was collected by centrifugation at 14,000 rpm in a SA600 rotor for 30 min. The supernatant was adjusted to 20 mM Tris-Cl, pH 8.0, snap frozen, and stored at −80°C. STxB was purified from the supernatant using mono Q with elution by increasing concentrations of NaCl. The protein was concentrated using Spin-X UF concentrators (Corning, Corning, NY). Purified STxB was tagged with Alexa Fluor 555 (Invitrogen, Carlsbad, CA) using manufacturer's protocols.

STxB binding assays

GST-tagged GPP130 constructs, GST-only control, and His-tagged STxB constructs were bacterially purified using standard methods (Mukhopadhyay and Linstedt, 2012). GST-proteins were dialyzed into phosphate-buffered saline (PBS), pH 7.3. His-tagged STxB was eluted in 50 mM NaH_2PO4, 300 mM NaCl, 250 mM imidazole, and 0.1% β-mercaptoethanol. The pH of the eluted His-STxB was adjusted to 7.3 using 1.7 μl of concentrated HCl per 100 μl of elute. Binding assays were performed in 100-μl reactions in PBS with 0.1% Triton X-100. We used 5 μM GST proteins and 0.4 μM STxB. GST-proteins and STxB were mixed and incubated at 4°C for 1 h with constant rotation, followed by addition of 5 μl of glutathione–agarose beads for another hour. Beads were then recovered by pulse spin, rapidly washed two times with PBS plus 0.1% Triton X-100 and once with PBS only, resuspended in reducing sample buffer, and analyzed by SDS–PAGE and Coomassie staining.

STx2B binding assays

Untagged STx2B was purified using a protocol similar to that used for the purification of untagged STxB (Mukhopadhyay and Linstedt, 2012). Briefly, a washed cell pellet from a 1-l culture was resuspended in 30 ml of ice-cold water with 10 μg/ml leupeptin, 10 μg/ml pepstatin, and 1 mM PMSF and, after 10 min on ice, a supernatant was collected by centrifugation at 14,000 rpm in a SA600 rotor for 30 min. The supernatant was adjusted to 20 mM Tris-Cl, pH 8.0, snap frozen, and stored at −80°C. STx2B was purified from the supernatant using a Q-column. Two milliliters of Q-Sepharose Fast Flow beads (GE Health Care Life Sciences, Pittsburgh, PA) was washed two times with 10 mM Tris-Cl, pH 8.0, and poured into a column. The supernatant was then added to the column and allowed to flow through with gravity. The column was washed with

25 ml of 10 mM Tris-Cl, pH 8.0. Bound proteins were sequentially eluted with buffer containing 10 mM Tris-Cl, pH 8.0, and increasing concentrations of NaCl (50, 100, 200, and 300 mM). STx2B eluted at 100 mM NaCl. The protein was concentrated using Spin-X UF concentrators (Corning). Binding assays were then performed using 5 µM GST proteins and 0.4 µM ST2xB exactly as described for the STxB proteins.

Transport assays

Transport of STxB was assayed essentially as described (Mukhopadhyay and Linstedt, 2012). HeLa cells were first transfected with untagged or GFP-tagged Gb3 synthase plasmid to reduce cell-to-cell variation in surface Gb3 levels (Shin *et al.*, 2009). The synthase was well localized to the Golgi and did not affect Golgi morphology or the kinetics of retrograde transport. After 2 d, the cultures were treated with or without 500 µM Mn for 4 h. After Mn treatment, cultures were washed three times in ice-cold PBS, incubated with 4 µg/ml STxB that had been fluorescently labeled with Alexa Fluor 555 in MEM at 4°C for 30 min, washed three more times in cold PBS, and transferred to regular medium at 37°C with or without 500 µM Mn for 30 min unless indicated otherwise. Cultures were then fixed using paraformaldehyde (3%) and processed for microscopy. To determine whether expression of GPP130 constructs could rescue STxB trafficking, cells were cotransfected with untagged Gb3 synthase and the indicated GPP130-GFP plasmids 2 d before the transport assay and treated with 500 µM Mn for 4 h, and the transport assay was then performed exactly as described. STx2B transport assays were performed exactly like those described for STxB, except that 3 µg/ml STx2 holotoxin was used. Assays comparing the transport of Alexa Fluor 555–labeled, untagged, wild type and $H_{78}A$-$N_{79}A$ STxB were performed as described with two differences: cells were transfected with GFP-tagged Gb3 synthase, and there was no Mn treatment.

STxB structure

Depictions of the crystal structure of STxB were derived using the algorithms of the ModBase server (http://modbase.compbio.ucsf.edu/modbase-cgi/index.cgi; Pieper *et al.*, 2006).

Image analysis

Immunofluorescence images were analyzed using ImageJ (National Institutes of Health, Bethesda, MD) essentially as described (Mukhopadhyay *et al.*, 2010; Mukhopadhyay and Linstedt, 2011, 2012). For fluorescence measurements in cells, average value projections were created from individual *Z*-stacks. Background for each image was then calculated for a region outside the cells using the Analyze-Measure functions of ImageJ and subtracted using Process-Math-Subtract. Total STxB or STx2 fluorescence per cell was then measured by outlining the cell using the freehand tool of ImageJ and Analyze-Measure. Temporary image adjustments were used to ensure accuracy of the outlining, but all measurements were made after reverting to original values. To measure Golgi fluorescence of STxB and STx2 in control cells, we demarcated the Golgi area using the staining of endogenous GPP130 and measured toxin fluorescence in this area. In Mn-treated cells one of two procedures were followed. In experiments in which GFP-tagged, Mn-insensitive GPP130 constructs were expressed, the GFP staining was used to demarcate the Golgi. The GFP-tagged GPP130 constructs contain a Golgi localization determinant and are well targeted to the Golgi (Mukhopadhyay *et al.*, 2010; Mukhopadhyay and Linstedt, 2012). In Mn-treated cells that did not express GFP-GPP130, brightness, contrast, and threshold values for the GPP130 channel were enhanced to enable detection of the low level of residual Golgi-localized GPP130.

Gel analysis

Coomassie-stained gels were analyzed using Image Gauge software (Fujifilm, Valhalla, NY). For each assay, binding of STxB or STx2B to GST only was considered background and subtracted from the binding to GST-GPP130. This specific binding was then expressed as percentage of total extrapolated from the value of the fraction of STxB or STx2 serving as a loading control.

Statistical analyses

All findings presented were replicated in three or more independent experiments. Statistical analyses were performed using Prism 6 software (GraphPad Software, La Jolla, CA). Comparisons between two groups were performed using two-tailed Student's *t* test assuming equal variances. Multiple group comparison at the same time was done using single-factor analysis of variance (ANOVA) with the Tukey–Kramer post hoc test. In general, $p < 0.05$ was considered significant, and the determined *p* values are provided in the figure legends. Asterisks in graphs, wherever present, denote statistically significant differences.

ACKNOWLEDGMENTS

We thank Semawit Gebrehiwot for preliminary work on the project and Collin Bachert for technical assistance and help with the manuscript. Tina Lee, Manoj Puthenveedu, and Jeffrey Brodsky (University of Pittsburgh, Pittsburgh, PA) provided feedback on the manuscript. This work was supported by National Institutes of Health Grants R01 GM-084111 (to A.D.L.) and K99/R00 ES-020844 (to S.M.).

REFERENCES

Aschner M, Erikson KM, Herrero Hernandez E, Tjalkens R (2009). Manganese and its role in Parkinson's disease: from transport to neuropathology. Neuromol Med 11, 252–266.

Bachert C, Lee TH, Linstedt AD (2001). Lumenal endosomal and Golgi-retrieval determinants involved in pH-sensitive targeting of an early Golgi protein. Mol Biol Cell 12, 3152–3160.

Beddoe T, Paton AW, Le Nours J, Rossjohn J, Paton JC (2010). Structure, biological functions and applications of the AB5 toxins. Trends Biochem Sci 35, 411–418.

Boerlin P, McEwen SA, Boerlin-Petzold F, Wilson JB, Johnson RP, Gyles CL (1999). Associations between virulence factors of Shiga toxin-producing *Escherichia coli* and disease in humans. J Clin Microbiol 37, 497–503.

Bretscher MS, Munro S (1993). Cholesterol and the Golgi apparatus. Science 261, 1280–1281.

Burk C, Dietrich R, Acar G, Moravek M, Bulte M, Martlbauer E (2003). Identification and characterization of a new variant of Shiga toxin 1 in *Escherichia coli* ONT:H19 of bovine origin. J Clin Microbiol 41, 2106–2112.

Chinnapen DJ *et al.* (2012). Lipid sorting by ceramide structure from plasma membrane to ER for the cholera toxin receptor ganglioside GM1. Dev Cell 23, 573–586.

Falguieres T, Mallard F, Baron C, Hanau D, Lingwood C, Goud B, Salamero J, Johannes L (2001). Targeting of Shiga toxin B-subunit to retrograde transport route in association with detergent-resistant membranes. Mol Biol Cell 12, 2453–2468.

Fontaine A, Arondel J, Sansonetti PJ (1988). Role of Shiga toxin in the pathogenesis of bacillary dysentery, studied by using a Tox- mutant of *Shigella* dysenteriae 1. Infect Immun 56, 3099–3109.

Gannon VP, Teerling C, Masri SA, Gyles CL (1990). Molecular cloning and nucleotide sequence of another variant of the *Escherichia coli* Shiga-like toxin II family. J Gen Microbiol 136, 1125–1135.

Johannes L, Popoff V (2008). Tracing the retrograde route in protein trafficking. Cell 135, 1175–1187.

Johannes L, Wunder C (2011). Retrograde transport: two (or more) roads diverged in an endosomal tree. Traffic 12, 956–962.
Keusch GT, Jacewicz M (1977). The pathogenesis of *Shigella* diarrhea. VI. Toxin and antitoxin in *Shigella flexneri* and *Shigella sonnei* infections in humans. J Infect Dis 135, 552–556.
Kotloff KL, Winickoff JP, Ivanoff B, Clemens JD, Swerdlow DL, Sansonetti PJ, Adak GK, Levine MM (1999). Global burden of *Shigella* infections: implications for vaccine development and implementation of control strategies. Bull World Health Org 77, 651–666.
Ling H, Boodhoo A, Hazes B, Cummings MD, Armstrong GD, Brunton JL, Read RJ (1998). Structure of the Shiga-like toxin I B-pentamer complexed with an analogue of its receptor Gb3. Biochemistry 37, 1777–1788.
Linstedt AD, Mehta A, Suhan J, Reggio H, Hauri HP (1997). Sequence and overexpression of GPP130/GIMPc: evidence for saturable pH-sensitive targeting of a type II early Golgi membrane protein. Mol Biol Cell 8, 1073–1087.
Mallard F, Antony C, Tenza D, Salamero J, Goud B, Johannes L (1998). Direct pathway from early/recycling endosomes to the Golgi apparatus revealed through the study of Shiga toxin B-fragment transport. J Cell Biol 143, 973–990.
Mohawk KL, O'Brien AD (2011). Mouse models of *Escherichia coli* O157:H7 infection and Shiga toxin injection. J Biomed Biotechnol 2011, 258185.
Mukhopadhyay S, Bachert C, Smith DR, Linstedt AD (2010). Manganese-induced trafficking and turnover of the *cis*-Golgi glycoprotein GPP130. Mol Biol Cell 21, 1282–1292.
Mukhopadhyay S, Linstedt AD (2011). Identification of a gain-of-function mutation in a Golgi P-type ATPase that enhances Mn2+ efflux and protects against toxicity. Proc Natl Acad Sci USA 108, 858–863.
Mukhopadhyay S, Linstedt AD (2012). Manganese blocks intracellular trafficking of Shiga toxin and protects against Shiga toxicosis. Science 335, 332–335.
Nataro JP, Pickering LK (2006). Oski's Paediatrics: Principles and Practice, Philadelphia: Lippincott Williams & Wilkins.
O'Brien AD, Holmes RK (1987). Shiga and Shiga-like toxins. Microbiol Rev 51, 206–220.
O'Brien AD, Thompson MR, Gemski P, Doctor BP, Formal SB (1977). Biological properties of *Shigella flexneri* 2A toxin and its serological relationship to *Shigella dysenteriae* 1 toxin. Infect Immun 15, 796–798.
Pieper U *et al*. (2006). MODBASE: a database of annotated comparative protein structure models and associated resources. Nucleic Acids Res 34, D291–D295.
Reller ME, Griffin PM (2004). Infectious Diseases, Philadelphia: Lippincott Williams & Wilkins.
Schmitt CK, McKee ML, O'Brien AD (1991). Two copies of Shiga-like toxin II-related genes common in enterohemorrhagic *Escherichia coli* strains are responsible for the antigenic heterogeneity of the O157:H- strain E32511. Infect Immun 59, 1065–1073.
Shin IS, Ishii S, Shin JS, Sung KI, Park BS, Jang HY, Kim BW (2009). Globotriaosylceramide (Gb3) content in HeLa cells is correlated to Shiga toxin-induced cytotoxicity and Gb3 synthase expression. BMB Rep 42, 310–314.
Strockbine NA, Jackson MP, Sung LM, Holmes RK, O'Brien AD (1988). Cloning and sequencing of the genes for Shiga toxin from *Shigella dysenteriae* type 1. J Bacteriol 170, 1116–1122.
Tam P, Mahfoud R, Nutikka A, Khine AA, Binnington B, Paroutis P, Lingwood C (2008). Differential intracellular transport and binding of verotoxin 1 and verotoxin 2 to globotriaosylceramide-containing lipid assemblies. J Cell Physiol 216, 750–763.
Tesh VL, Burris JA, Owens JW, Gordon VM, Wadolkowski EA, O'Brien AD, Samuel JE (1993). Comparison of the relative toxicities of Shiga-like toxins type I and type II for mice. Infect Immun 61, 3392–3402.
Weinstein DL, Jackson MP, Samuel JE, Holmes RK, O'Brien AD (1988). Cloning and sequencing of a Shiga-like toxin type II variant from *Escherichia coli* strain responsible for edema disease of swine. J Bacteriol 170, 4223–4230.
Zhang W, Bielaszewska M, Friedrich AW, Kuczius T, Karch H (2005). Transcriptional analysis of genes encoding Shiga toxin 2 and its variants in *Escherichia coli*. Appl Environ Microbiol 71, 558–561.